A Journal of the Gesellschaft Deutscher Chemiker

Angewandte International Edition Chemie

GDCh

www.angewandte.org

Accepted Article

Title: Ultrasmall Zeolite L Crystals Prepared from Highly-Interdispersed Alkali-Silicate Precursors

Authors: Rui Li, Noemi Linares, James G. Sutjianto, Aseem Chawla, Javier Garcia Martinez, and Jeffrey D. Rimer

To be cited as: *Angew. Chem. Int. Ed.* 10.1002/anie.201805877
Angew. Chem. 10.1002/ange.201805877

Link to VoR: http://dx.doi.org/10.1002/anie.201805877
http://dx.doi.org/10.1002/ange.201805877

WILEY-VCH

10.1002/anie.201805877

WILEY-VCH

COMMUNICATION

Ultrasmall Zeolite L Crystals Prepared from Highly-Interdispersed Alkali-Silicate Precursors

Rui Li†[a], Noemi Linares†[b], James G. Sutjianto[a], Aseem Chawla[a], Javier Garcia-Martinez*,[b], and Jeffrey D. Rimer*,[a]

Abstract: The preparation of nanosized zeolites is critical for applications where mass transport limitations within microporous networks hinder their performance. Oftentimes the ability to generate ultrasmall zeolite crystals is dependent upon the use of expensive organics with limited commercial relevance. Here, we report the generation of zeolite L crystals with uniform sizes less than 30 nm using a facile, organic-free method. Time-resolved analysis of precursor assembly and evolution during nonclassical crystallization highlights key differences among silicon sources. Our findings reveal that a homogenous dispersion of potassium ions throughout silicate precursors is critical to enhancing the rate of nucleation and facilitating the formation of ultrasmall crystals. Intimate contact between the inorganic structure-directing agent and silica leads to the formation of a metastable nonporous phase, identified as $KAlSi_2O_6$, which undergoes an intercrystalline transformation to zeolite L. The presence of highly-interdispersed alkali-silicate precursors is seemingly integral to a reduced zeolite induction time and may facilitate the development of ultrasmall crystals. Given the general difficulty of achieving nanosized crystals in zeolite synthesis, it is likely that using well-dispersed precursors does not have the same effect on all framework types; however, in select cases it may provide an alternative strategy for optimizing zeolite synthesis.

Zeolites are microporous aluminosilicates that find extensive use as commercial catalysts in (petro)chemical industries, adsorbents for gas separations, and as ion-exchange materials for water purification owing to their unique physicochemical properties (i.e., porosity, acidity, and hydrothermal stability). In these and other applications, achieving optimal performance of materials is often tied to the generation of nanosized crystals. Examples include the preparation of ultrasmall (<20 nm) crystallites[1] and 2-dimensional (2D) materials (ca. 3 nm thick nanosheets)[2] where the diffusion path length in microporous channels is limited to a few unit cells of the crystal, thereby reducing internal mass transport limitations. Fewer than 20 zeolite framework types have been synthesized with dimensions less than 100 nm.[3] Methods to prepare ultrasmall zeolites are generally hindered by a lack of knowledge regarding zeolite growth that can, in turn, guide the *a priori* selection of synthesis conditions. A critical, albeit not fully explored, synthesis parameter is the selection of silicon and/or aluminum sources, which can impact the kinetics of crystallization and alter crystal properties. For example, it has been reported that the judicious selection of sources can significantly reduce the size of ZSM-5 (MFI) crystals.[4] Similar findings have been reported for silicalite-1 (MFI)[5], zeolite L (LTL)[6], mordenite (MOR)[7], zeolite A (LTA)[8], zeolite X (FAU)[9], and analcime (ANA).[10] Moreover, it has been demonstrated for MCM-22 (MWW) that the induction period is influenced by source selection.[11] Despite significant efforts to elucidate the role of sources in zeolite synthesis, many fundamental questions remain unanswered.

Prior studies reveal that zeolites grow from mixtures comprised of amorphous precursors that range in complexity from (alumino)silicate oligomers[12] to disordered nanoparticles, colloidal aggregates, or gels.[13] It has been demonstrated by our group[14] and others[15] that precursors assemble and evolve in both size and structure during the induction period. The roles of precursors in zeolite nucleation, as well as their potential function as growth units during crystallization, have been postulated; however, these processes are generally not well understood for the vast majority of zeolites.[13b, 14] Moreover, quantitative relationships between the physicochemical properties of source reagents[16] and their corresponding amorphous precursors[14] have yet to be established. It is reasonable to assume that the choice of silicon and aluminum sources can impact the pathways of zeolite crystallization, either through nonclassical routes involving growth by the attachment of amorphous precursors or via classical pathways governed by monomer addition.[17]

In this study, we examine the impact of alkali distribution in amorphous precursors of zeolite L (LTL), a one-dimensional large pore zeolite with cylindrical morphology (Figure S1). Zeolite L is used commercially as a catalyst and is a promising material for applications in photonics[18] and drug delivery[19]. Unlike the vast majority of zeolite frameworks, zeolite L is prepared without organics using potassium as the sole structure-directing agent (SDA).[20] Our findings indicate that the intimate contact between the potassium ions and the silicon source within amorphous precursors enhances the rate of nucleation and leads to the formation of ultrasmall crystals (ca. 20 nm). Parametric studies of zeolite L synthesis using combinations of Si and Al sources (Table S1) reveal that the former have more pronounced effects on crystal phase purity and size (Figure S2). The nominal molar composition of growth mixtures in this study is 0.5 Al_2O_3:20 SiO_2:10.2 K_2O:1030 H_2O where aluminum sulfate was used to set the overall Si/Al ratio (or SAR) at 20.[20] Under these conditions, LTL was obtained. In the case of potassium silicate, there is additional potassium (4 K^+ per SiO_2) and syntheses yield an appreciable fraction of merlinoite (MER), which is a common zeolite impurity.[21] In order to avoid the formation of MER, synthesis mixtures with potassium silicate are prepared at higher Si content using a molar ratio of 0.5 Al_2O_3:36.4 SiO_2:10.2 K_2O: 1030 H_2O (SAR = 36 and 88% additional K^+; referred to as the *high SAR* recipe), keeping all other conditions fixed.

Syntheses of zeolite L tend to produce ca. 3 µm crystals (Figure S1). Protocols for generating small zeolite L crystals often require long crystallization time (e.g., 18 – 48 h)[22] and/or the use of microwave synthesis[22b] or unconventional reagents (e.g., aluminum foil[23] and rice husk[24]) that are not readily employed in commercial processes. In this study, we observe that potassium silicate yields ultrasmall zeolite L crystals with average sizes that are nearly one-half the smallest reported size[25] (Table S2 and Figures S3 – S8). Scanning electron microscopy (SEM) images indicate sizes of ca. 65 nm (Figure 1 A); however, transmission electron microscopy (TEM) reveal that these larger particles are clusters of small individual crystals (Figure 1 B) with a [100]

[a] Dr. R. Li, J.G. Sutjianto, A. Chawla, Prof. J.D. Rimer
Department of Chemical and Biomolecular Engineering
University of Houston
Houston, TX 77204, USA
E-mail: jrimer@central.uh.edu
[b] Dr. N. Linares, Prof. J. Garcia-Martinez
Molecular Nanotechnology Lab
Department of Inorganic Chemistry
University of Alicante
03690 Alicante, Spain
E-mail: j.garcia@ua.es

Supporting information for this article is given via a link at the end of the document.

10.1002/anie.201805877

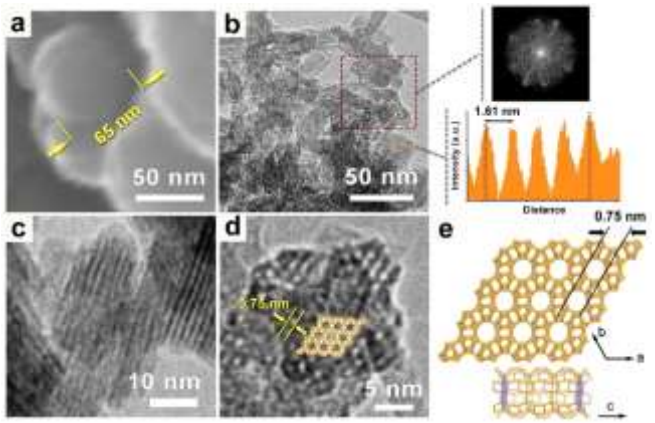

Figure 1. (A) SEM image showing clusters (ca. 65 nm) of zeolite L crystals obtained from potassium silicate (sample N-9 in Table S2). (B) Low magnification TEM image showing clusters are comprised of individual crystals. Inset: (top) The Fast Fourier Transform (FFT) of the selected area (red square) produces a halo due to the polycrystalline nature of the nanoparticles. (bottom) Line scan along the orange line reveals lattice fringes with an interplanar spacing of 1.61±0.07 nm (Figure S10). (C) High magnification TEM image of ultrasmall zeolite L crystals with distinct lattice fringes. (D) TEM image capturing the hexagonal arrangement of 0.75 nm diameter pores in the [001] direction (an LTL structure is overlaid for reference). (E) Projection of the LTL framework in the *c*-direction illustrating the one-dimensional (1-D) channels and hexagonal crystal structure (*P6/mmm*) with unit cell parameters $a = b = 1.81$ and $c = 0.76$ nm.

length of 32 ± 5 nm and a [100] width of 11 ± 2 nm(Figure S13 C and D). These sizes are consistent with those estimated from peak broadening in powder X-ray diffraction (XRD) patterns using the Scherrer equation (i.e., analysis of peaks at $2\theta = 30 – 50°$ in Figure S9 A estimates an average crystal size of 25 ± 9 nm). To account for the anistropy of zeolite L crystal shape, we also analyzed XRD patterns by the Williamson–Hall method[26] using the h00 and 00l reflections (due to the prismatic shape of LTL crystals, see Figure S9 B), which results in a crystal length and width of 31.5 and 18.2 nm, respectively, similar to the sizes obtained by TEM. High resolution TEM images resolved lattice fringes (Figure 1 C) with an interplanar spacing of 1.61 ± 0.07 nm (Figure 1 B, inset), which results in a cell dimension of 1.86 ± 0.08 nm, very similar to the *a* and *b* unit cell dimensions of LTL. Low magnification images (Figure S13) confirm the narrow size distribution of ultrasmall zeolite L crystals, as well as the absence of amorphous material and large crystals in the sample. Moreover, transmission electron micrographs capture crystals along the *c*-axis (Figure 1 D) with a hexagonal arrangement of 0.75 nm channels, consistent with the crystal structure of LTL (Figure 1 E and Figures S11 and S12).

Zeolite L crystals are often reported in literature as *nanoclusters*[25, 27] that are either aggregates of smaller crystallites or single crystals with protrusions attributed to defects (e.g., intergrowths) and/or the byproduct of nonclassical growth (e.g., crystallization by particle attachment). It is more challenging to measure the crystal size distribution when clusters are comprised of crystallographically aligned particles. Moreover, aggregates of aligned crystals likely impose longer internal diffusion path lengths compared to individual nanocrystals within the cluster.[28] A notable finding of this study is that the clusters of ultrasmall zeolite L crystals are comprised of randomly oriented nanoparticles, as confirmed by extensive TEM analysis. Indeed, FFT patterns (Figure 1 B, inset) reveal a disparity of crystal alignment, suggesting the clusters are a collection of individual crystals with incongruent orientations rather than aggregates of *c*-oriented crystals. Low magnification TEM images (Figure S13) also reveal a high degree of crystallinity without residual amorphous product detected in the micrographs. Indeed, the preparation of ultrasmall zeolite L allows for complete crystallization, which differs from approaches where nanosized zeolites are obtained by quenching syntheses at short heating times (i.e., terminating growth once crystals reach a desirable size). Disadvantages of the latter approach are low yields and residual amorphous product that is both inefficient and wasteful.

In addition to producing ultrasmall zeolite L crystals, we observed that potassium silicate significantly shortens the crystallization time (3 – 4 h) compared to alternative sources (e.g., 10 h for colloidal silica). Potential explanations for the distinctiveness of potassium silicate are (i) the increased Si content of the high SAR recipe and (ii) the corresponding increase in potassium content introduced into the growth mixture. To test the former, we performed experiments with colloidal silica where the SAR of synthesis mixture was increased to the level of potassium silicate (Figure S14). High SAR syntheses with colloidal silica yield an amorphous product, even after 7 days of heating (Figure S14 A). The effect of potassium content was evaluated by adding KBr salt to the high SAR growth mixture prepared with colloidal silica; however, the presence of additional K^+ ions shifted the product to non-zeolite inorganic crystals (Figure S14 B). These observations suggest a third possibility for the effects of potassium silicate: (iii) the close proximity between K^+ ions and the silicon source (i.e., a high degree of interdigitation).

To test this hypothesis, we selected two silicon sources (potassium silicate and colloidal silica) and evaluated potential differences in their spatial distribution of potassium using FE-SEM-EDX elemental mapping. Analysis of as received potassium silicate shows the overlay of elements (Figure 2 A) with individual mappings of K (Figure 2 B, blue) and Si (Figure 2 C, red) shown separately. These images indicate that, as expected, K^+ is evenly distributed throughout the particles. In order to determine if K^+ is homogeneously dispersed throughout the particle interior, we analyzed a cross-sectional area of a potassium silicate slice (Figure 2 D – F), which clearly shows K^+ homogeneously distributed throughout the sample. On the contrary, similar analyses of colloidal silica soaked in a 2 M $KBr_{(aq)}$ solution for 1 to 7 days and extracted for analysis shows that K^+ is marginally retained on the exterior surface, but is not contained within the particle interior (Figure 2 G – I). A similar result was obtained for fumed silica soaked in $KBr_{(aq)}$ for 1 day (see Figure S15). The results of elemental mapping indicate a more intimate contact between alkali and silica in potassium silicate. Idealized distributions of potassium in each silicon source are illustrated in Figure 2 J, showing that potassium silicate produces a highly-interdispersed alkali-silicate precursor. In order for colloidal silica particles to achieve a similar spatial distribution of K^+ ions, a considerable degree of silica must dissolve and reprecipitate.

In zeolite synthesis, the addition of a silicon source to alkaline media can result in little dissolution owing to low silica solubility and the deposition of alumina on exterior surfaces of silicates,[16] which decreases the rate of precursor dissolution. This leads to heterogeneous particles comprised of isolated silica and alumina domains where alkali metal distribution has not been sufficiently addressed. For potassium silicate and other alkali metal silicates, $M_2O \cdot nSiO_2$ (M = Li^+, Na^+, K^+, etc.), their solubility in water decreases with increasing silica content (in this study we use potassium silicate with n = 4).[29] We postulate that differences in K^+ distribution among various silicon sources impact precursor assembly and evolution, with concomitant effects on zeolite L nucleation. Prior studies have established that zeolite L crystallization from colloidal silica involves the formation of amorphous *worm-like particles* (WLPs).[14] These precursors are widely observed in zeolite synthesis[15, 30] and exhibit a morphology that suggests they assemble (or coalescence) from the original colloidal silica particles, which remain largely undissolved during the early stages of hydrothermal treatment. The spheroidal domains of WLPs derived from colloidal silica (Figure 3 A) and fumed silica (Figure 3 B) are similar. These domains are seemingly fused together as a result of variances in

10.1002/anie.201805877

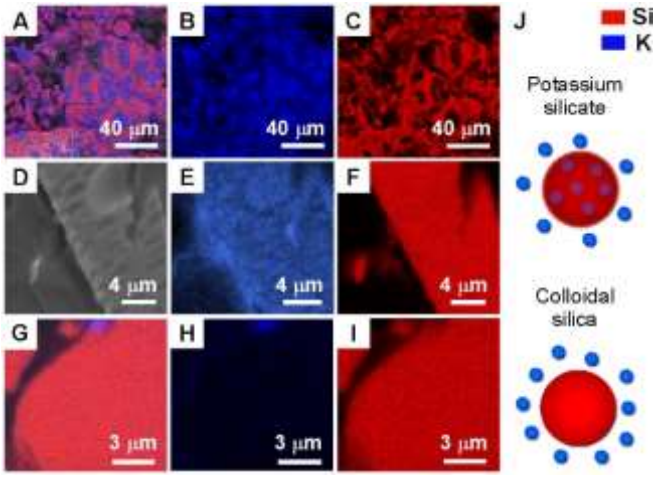

Figure 2. SEM-EDX elemental mapping of potassium silicate particles as powder without modification (A-C) and its corresponding ultramicrotomed form (D-F) reveal dispersed K^+ throughout the exterior and interior of the silicon source, respectively. (G – I) Similar elemental mapping for ultramicrotomed colloidal silica after soaking in $KBr_{(aq)}$ solution for 1 day reveals that there are traces of potassium on the exterior surface of colloidal silica particles, but none is observed within the particle interior (note: the same result was observed after 7 days). A similar outcome was observed for fumed silica soaked in $KBr_{(aq)}$ for 1 day (see Figure S15). (J) Illustrative renderings of potassium distribution in two silicon sources: potassium silicate (top) and colloidal silica (bottom). Color coding: K (blue) and Si (red).

silica solubility induced by surface curvature, analogous to the Laplace pressure of a curved gas-liquid interface.[31] The exact role of WLPs in the amorphous-to-crystalline transition of precursors to zeolite L (Figure S16) is not well understood.

Our findings indicate that the choice of silica greatly impacts the size and morphology of amorphous precursors. WLPs formed from colloidal and fumed silica are similar, despite large differences in their original particle sizes (25 and 70 nm, respectively, see Figure S17). Conversely, precursors of potassium silicate do not evolve into WLPs. The latter remain as small particles with ill-defined morphology (Figure 3 C). All reagents yield sols with alumina on the exterior surfaces of silica particles (as reported in our previous study).[14, 16] An exception is fumed silica, which initially yields a viscous gel that gradually decomposes to a liquid sol after rigorous stirring (Figure S18). During room temperature aging, time-resolved changes in supernatant pH (Figure 3 D) and ionic conductivity (Figure S19) reveal distinct differences among silicon sources, which likely reflect a disparity of precursor dissolution. As silicates dissolve, the depletion of hydroxide ions reduces solution pH and ionic conductivity (i.e., $\equiv Si - O - Si \equiv + OH^- \rightarrow \equiv SiO^- + HOSi \equiv$). It has been shown that the rate of silicate dissolution is correlated to its microstructure. For example, amorphous particles dissolve much faster than crystalline materials (i.e., more dense silicates).[32] On this basis, we hypothesize that fumed silica and potassium silicate are comprised of less dense SiO_2 compared to colloidal silica (i.e., these amorphous sources likely differ in silica connectivity). Indeed, dissolution studies of each source in KOH solution using dynamic light scattering to track the temporal reduction in particle size reveals that fumed silica dissolves at an approximate 5-fold faster rate than that of colloidal silica (Figure S20). Similar measurements of potassium silicate were not possible owing to particle aggregation in DLS studies. Collectively, measurements of precursor dissolution are qualitatively consistent with the trends in Figure 3 D; however, such data cannot provide direct evidence for the putative differences in precursor microstructure.

Highly-interdispersed potassium and silica precursors dramatically reduce the rate of zeolite L nucleation. As shown in Figure 3 E, the induction time for potassium silicate is one-fourth that of colloidal silica and one-third that of fumed silica. Valtchev and coworkers observed similar reductions in zeolite L induction time, and proposed that the rapid diffusion of K^+ ions within precursors leads to faster nucleation.[27b] To test the hypothesis that a homogeneous distribution of K^+ within the silica precursor leads to more favorable kinetics of crystallization, we attempted to infuse fumed silica with additional potassium. To this end, we soaked as received fumed silica in 2 M $KBr_{(aq)}$ for one week with the anticipation that K^+ ions may diffuse into silica particles. Elemental analysis of K^+–infused (or "modified") fumed silica by FE-SEM-EDX (Figure 3 F) confirmed that K^+ ions are homogenously distributed throughout the particles after soaking (ca. 1 wt%). The high SAR recipe using modified fumed silica results in MER impurity; therefore, the Si content was increased further to an SAR of 50 in order to yield pure LTL crystals (Figure S21). This modified fumed silica growth mixture resulted in a much lower induction time (Figure 3 E), identical to that of potassium silicate. Moreover, syntheses employing potassium silicate and modified fumed silica yield similarly-sized zeolite L crystals (Figure S22), thereby confirming the importance of having well dispersed K^+ within the silica precursor to produce ultrasmall LTL crystals.

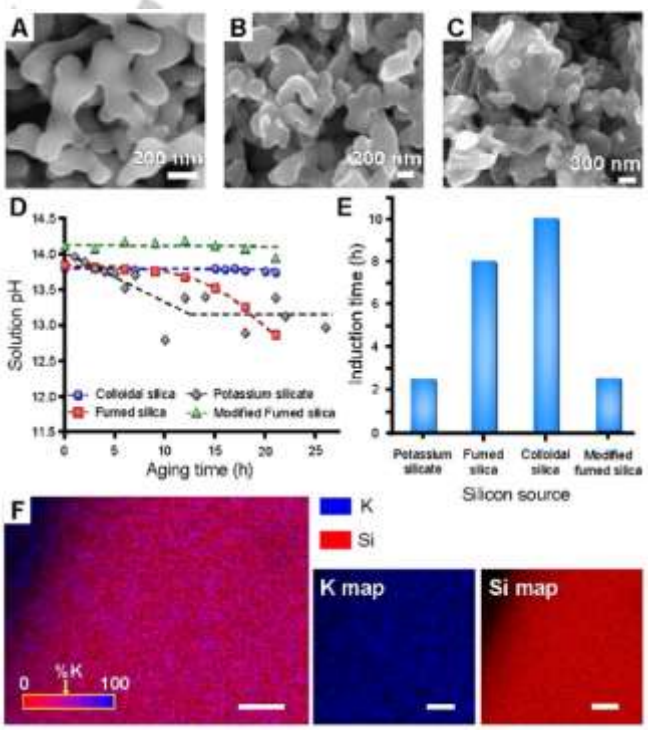

Figure 3. SEM images of precursors evolved from different silicon sources: (A) colloidal silica, (B) fumed silica, and (C) potassium silicate. (D) Temporal changes in solution pH during room temperature aging for four silicon sources: colloidal silica (blue circles), fumed silica (red squares), potassium silicate (grey diamonds) and modified fumed silica (green triangles). The compositions of growth mixtures and corresponding changes in solution conductivity are provided in Table S4 and Figure S19, respectively. Dashed lines are interpolations to guide the eye. (E) Induction times for zeolite L crystallization using growth mixtures at the same conditions, but prepared with different silicon sources. Times refer to the first appearance of Bragg peaks in powder XRD patterns. (F) FE-SEM-EDX elemental mapping of fumed silica exposed to 2 M $KBr_{(aq)}$ for 1 week. Callouts to the right depict single element maps. Scale bars equal 2 μm. Color coding: blue is K and red is Si.

10.1002/anie.201805877

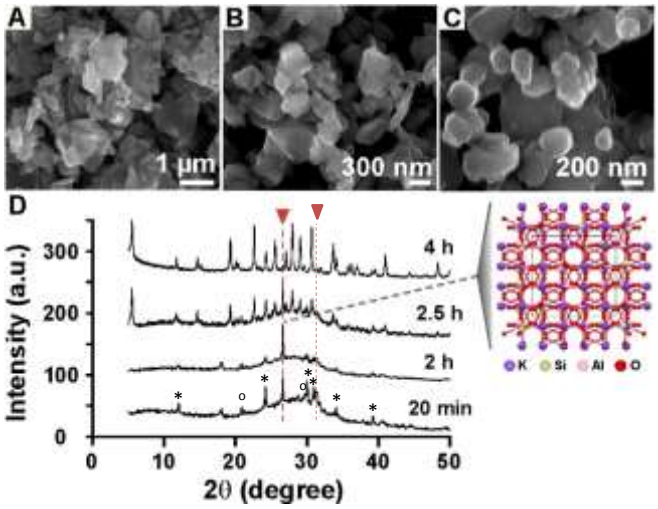

Figure 4. Time-resolved SEM images of solids extracted from a zeolite L growth mixture using potassium silicate. Images correspond to synthesis mixtures after hydrothermal treatment for (A) 20 min, (B) 2.5 h, and (C) 4 h. (D) Powder XRD patterns of the corresponding solid samples Peaks indexed to trace $KHCO_3$ (*) and K_2SO_4 (º) are shown at short times. The presence of amorphous material and potassium aluminum silicate crystal impurity (arrows and dashed lines at 2θ = 26.7° and 31º) is observed during the first stages of zeolite crystallization. The same phenomenon occurs in growth mixtures derived from modified fumed silica (see Figure S25). Inset: crystal structure of potassium aluminosilicate, $KAlSi_2O_6$. Color coding: K is purple, Al is pink, Si is beige, and O is red.

The ability of highly-interdispersed alkali-silicate species to yield ultrasmall zeolite L crystals was investigated in more detail by monitoring the temporal evolution of precursors during crystallization. SEM images of solids extracted from a potassium silicate growth mixture after periodic times of hydrothermal treatment (Figure 4 A – C) reveal the absence of WLPs. Interestingly, the first Bragg peaks in powder XRD patterns (Figure S23) correspond to several inorganic crystalline phases, such as potassium sulfate, potassium hydrogen carbonate, and potassium aluminosilicate. Given that potassium salts are highly soluble in aqueous solution, simple washing with deionized (DI) water usually removes these phases. This was observed for all samples with the exception of those prepared using potassium silicate where residual $KHCO_3$, K_2SO_4, and $KAlSi_2O_6$ phases (Figure 4 D) could not be easily removed by two centrifuge/washing cycles. More rigorous separation steps (e.g., five centrifuge/washing cycles) were able to remove a majority of potassium salts (Figure S24), while potassium aluminosilicate, $KAlSi_2O_6$, was the remaining predominant phase in powder XRD patterns (Figure 4 D, inset).

Time-resolved XRD patterns reveal that amorphous material and $KAlSi_2O_6$ are precursors to zeolite L formation. The latter is the first crystal observed during early stages of hydrothermal treatment, and becomes a more dominant phase after 2 h of heating. There is no observable change in precursor size or morphology during the formation of $KAlSi_2O_6$ (Figure 4 A and 4 B), or during its transition to fully crystalline zeolite L (Figure 4 C). The formation of an intermediate (nonporous) crystalline phase and its subsequent transformation to a zeolite is not uncommon. Indeed, zeolites can be produced from aluminosilicate minerals, which are inexpensive sources of aluminum and/or silicon. Examples include potassium feldspar ($KAlSi_3O_8$)[33], kaolin ($Al_2Si_2O_5(OH)_4$)[34], coal fly ash[35], and boehmite (AlO(OH))[36], among others. Beyond the economic advantage of using these sources in zeolite synthesis, it is possible that minerals with highly-interdispersed alkali (e.g., feldspars such as microcline)[37] may lead to more rapid crystallization, similar to the effects of potassium silicate observed in this study.

The exact mechanism of zeolite L nucleation and growth is not well understood. Indeed, the abilty to characterize zeolite nucleation at a molecular level remains a significant challenge.[38] It is possible that amorphous precursors or species in solution play a significant role in nucleation, or potentially the potassium aluminosilicate phase despite the difference in crystal symmetry between $KAlSi_2O_6$ ($Ia\bar{3}d$, cubic) and zeolite L (*P6/mmm*, hexagonal). For instance, there may be structural similarities between the two crystals that could facilitate solid state rearrangement, although dissolution and reprecipitation of $KAlSi_2O_6$ is an essential pathway of zeolite L crystallization. It is reasonable to assume that potassium (i.e., the inorganic SDA) plays a key role wherein its homogeneous distribution throughout potassium silicate seemingly promotes the initial formation of $KAlSi_2O_6$. It remains to be determined if this metastable intermediate contributes to the shorter induction time and/or impedes the evolution of amorphous precursors to larger WLPs.

In summary, we have shown that the judicious selection of silicon sources and the distribution of K^+ throughout the assembled amorphous precursors significantly enhances the rate of zeolite L crystallization. The disorder-to-order transition that occurs from these mixtures result in the formation of metastable nonporous crystalline phases intermixed with amorphous particles that collectively serve as the predecessors to zeolite L nucleation. Precursors derived from potassium silicate differ from conventional suspensions of worm-like particles and yield ultrasmall crystals (ca. 20 nm), which are the smallest zeolite L crystallites reported in literature. Preparation of ultrasmall zeolite L crystals is seemingly connected with the homogeneous distribution of alkali throughout the silicate precursor. Given the common use of potassium as an inorganic structure-directing agent for a number of zeolites, the facile and effective method of generating interdispersed alkali-silicate precursors may prove to be applicable to other framework types as a platform to tailor the kinetics of zeolite formation and the properties of crystalline products.

Acknowledgements

J.D.R. acknowledges support primarily from the U.S. Department of Energy, Office of Science, Office of Basic Energy Sciences under Award Number DE-SC0014468. Additional support was provided by the Welch Foundation (Award E-1794). N.L. acknowledges support from the University of Alicante under the project GRE15-07. We thank C. Almansa and V. López for assistance with the microscopic analyses.

Keywords: zeolite L • nonclassical crystallization • catalyst • amorphous precursor • intercrystalline transformation

[1] a) E.-P. Ng, D. Chateigner, T. Bein, V. Valtchev, S. Mintova, Science 2012, 335, 70-73; b) H. Awala, J.-P. Gilson, R. Retoux, P. Boullay, J.-M. Goupil, V. Valtchev, S. Mintova, Nature Materials 2015, 14, 447.

[2] M. Y. Jeon, D. Kim, P. Kumar, P. S. Lee, N. Rangnekar, P. Bai, M. Shete, B. Elyassi, H. S. Lee, K. Narasimharao, S. N. Basahel, S. Al-Thabaiti, W. Xu, H. J. Cho, E. O. Fetisov, R. Thyagarajan, R. F. DeJaco, W. Fan, K. A. Mkhoyan, J. I. Siepmann, M. Tsapatsis, Nature 2017, 543, 690.

[3] V. Valtchev, L. Tosheva, Chemical Reviews 2013, 113, 6734-6760.

[4] H. Liu, G. Z. Liu, X. W. Zhang, D. D. Zhao, L. Wang, Microporous and Mesoporous Materials 2017, 244, 164-170.

[5] S. Mintova, V. Valtchev, Microporous Mesoporous Mat. 2002, 55, 171-179.

[6] Y.-J. Lee, J. S. Lee, K. B. Yoon, Microporous and Mesoporous Materials 2005, 80, 237-246.

[7] J. Warzywoda, A. G. Dixon, R. W. Thompson, A. Sacco, S. L. Suib, Zeolites 1996, 16, 125-137.
[8] C. I. Round, S. J. Hill, K. Latham, C. D. Williams, Microporous Materials 1997, 11, 213-225.
[9] K. E. Hamilton, E. N. Coker, A. Sacco, A. G. Dixon, R. W. Thompson, Zeolites 1993, 13, 645-653.
[10] G. S. Wiersema, R. W. Thompson, Journal of Materials Chemistry 1996, 6, 1693-1699.
[11] Y. J. Wu, X. Q. Ren, Y. D. Lu, J. Wang, Microporous and Mesoporous Materials 2008, 112, 138-146.
[12] S. L. Burkett, M. E. Davis, Chemistry of Materials 1995, 7, 1453-1463.
[13] aS. Mintova, N. H. Olson, V. Valtchev, T. Bein, Science 1999, 283, 958-960; bA. I. Lupulescu, J. D. Rimer, Science 2014, 344, 729-732.
[14] M. Kumar, R. Li, J. D. Rimer, Chemistry of Materials 2016, 28, 1714-1727.
[15] N. Ren, B. Subotić, J. Bronić, Y. Tang, M. Dutour Sikirić, T. Mišić, V. Svetličić, S. Bosnar, T. Antonić Jelić, Chemistry of Materials 2012, 24, 1726-1737.
[16] M. D. Oleksiak, J. A. Soltis, M. T. Conato, R. L. Penn, J. D. Rimer, Chemistry of Materials 2016, 28, 4906-4916.
[17] J. J. De Yoreo, P. U. P. A. Gilbert, N. A. J. M. Sommerdijk, R. L. Penn, S. Whitelam, D. Joester, H. Zhang, J. D. Rimer, A. Navrotsky, J. F. Banfield, A. F. Wallace, F. M. Michel, F. C. Meldrum, H. Cölfen, P. M. Dove, Science 2015, 349.
[18] B. Schulte, M. Tsotsalas, M. Becker, A. Studer, L. De Cola, Angewandte Chemie International Edition 2010, 49, 6881-6884.
[19] H. Lülf, A. Bertucci, D. Septiadi, R. Corradini, L. De Cola, Chemistry – A European Journal 2014, 20, 10900-10904.
[20] A. I. Lupulescu, M. Kumar, J. D. Rimer, Journal of the American Chemical Society 2013, 135, 6608-6617.
[21] J. C. Quirin, L. T. Yuen, S. I. Zones, Journal of Materials Chemistry 1997, 7, 2489-2494.
[22] a) A. Kharchenko, O. I. Lebedev, V. Zholobenko, V. de Waele, S. Mintova, The Journal of Physical Chemistry C 2016, 120, 26300-26308; b) S. Laurent, E. P. Ng, C. Thirifays, L. Lakiss, G. M. Goupil, S. Mintova, C. Burtea, E. Oveisi, C. Hebert, M. de Vries, M. M. Motazacker, F. Rezaee, M. Mahmoudi, Toxicology Research 2013, 2, 270-279.
[23] M. Tsapatsis, M. Lovallo, T. Okubo, M. E. Davis, M. Sadakata, Chemistry of Materials 1995, 7, 1734-1741.
[24] K.-H. Tan, H.-Y. Cham, H. Awala, T. C. Ling, R. R. Mukti, K.-L. Wong, S. Mintova, E.-P. Ng, Nanoscale Research Letters 2015, 10, 253.
[25] M. C. Lovallo, M. Tsapatsis, T. Okubo, Chemistry of Materials 1996, 8, 1579-1583.
[26] a) A. W. Burton, K. Ong, T. Rea, I. Y. Chan, Microporous Mesoporous Mat. 2009, 117, 75-90; b) V. D. Mote, Y. Purushotham, B. N. Dole, J. Theor. Appl. Phys. 2012, 6, 6; c) L. Gartzia-Rivero, J. Banuelos, U. Izquierdo, V. L. Barrio, K. Bizkarra, J. F. Cambra, I. Lopez-Arbeloa, Part. Part. Syst. Charact. 2014, 31, 110-120.
[27] a) M. Tsapatsis, M. Lovallo, M. E. Davis, Microporous Materials 1996, 5, 381-388; b) L. Itani, K. N. Bozhilov, G. Clet, L. Delmotte, V. Valtchev, Chem.-Eur. J. 2011, 17, 2199-2210.
[28] S. Mintova, M. Jaber, V. Valtchev, Chem. Soc. Rev. 2015, 44, 7207-7233.
[29] H. H. Weldes, K. R. Lange, Industrial and Engineering Chemistry 1969, 61, 29-&.
[30] A. Chawla, R. Li, R. Jain, R. J. Clark, J. G. Sutjianto, J. C. Palmer, J. D. Rimer, Molecular Systems Design & Engineering 2018, 3, 159-170.
[31] R. K. Iler, The Chemistry of Silica: Solubility, Polymerization, Colloid and Surface Properties and Biochemistry of Silica, Wiley, 1979.
[32] J. D. Rimer, O. Trofymluk, A. Navrotsky, R. F. Lobo, D. G. Vlachos, Chemistry of Materials 2007, 19, 4189-4197.
[33] a) S. Q. Su, H. W. Ma, X. Y. Chuan, Adv. Powder Technol. 2016, 27, 139-144; b) J. Y. Yuan, J. Yang, H. W. Ma, Q. Q. Chang, ChemistrySelect 2017, 2, 10722-10726.
[34] a) D. Akolekar, A. Chaffee, R. F. Howe, Zeolites 1997, 19, 359-365; b) J. Zhu, Y. Cui, Y. Wang, F. Wei, Chem. Commun. 2009, 3282-3284.
[35] X. Querol, N. Moreno, J. C. Umana, A. Alastuey, E. Hernandez, A. Lopez-Soler, F. Plana, Int. J. Coal Geol. 2002, 50, 413-423.
[36] B. Herreros, J. Klinowski, J. Chem. Soc.-Faraday Trans. 1995, 91, 1147-1154.
[37] J. Y. Yuan, J. Yang, H. W. Ma, C. J. Liu, C. L. Zhao, RSC Adv. 2016, 6, 54503-54509.
[38] J. D. Rimer, M. Tsapatsis, MRS Bull. 2016, 41, 393-398.

10.1002/anie.201805877

WILEY-VCH

COMMUNICATION

Fast Track. A new method of preparing nanosized zeolite L crystals from silicates comprised of highly-interdispersed potassium ions reveals that a uniform distribution of inorganic structure-directing agents can alter the pathway of zeolite crystallization and dramatically reduce synthesis time.

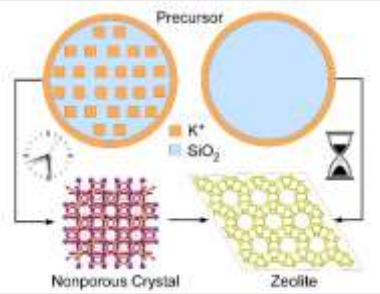

Dr. Rui Li, Dr. Noemi Linares, James G. Sutjianto, Aseem Chawla, Prof. Javier Garcia Martinez, and Prof. Jeffrey D. Rimer**

Page No. – Page No.

Ultrasmall Zeolite L Crystals Prepared from Highly-Interdispersed Alkali-Silicate Precursors